Theoret. Chim. Acta (Berl.) 57, 1–23 (1980)

THEORETICA CHIMICA ACTA

Original Investigations

An Improved LCAO SCF Method for Three-Dimensional Solids and Its Application to Polyethylene, Graphite, Diamond, and Boron Nitride

Peter G. Perkins, Ashok K. Marwaha, and James J. P. Stewart

Department of Pure and Applied Chemistry, University of Strathclyde, Glasgow G1 1XL, Scotland

An improved semi-empirical self-consistent scheme is described for calculating the band structures of three-dimensional solids. The basic level is that of CNDO theory. The non-orthogonality of the Bloch functions is recognised and allowance is made for all degrees of involvement of the overlap matrix. The calculation of the electron-repulsion integrals is formulated in a way suitable for solid-state problems. The method is tested on the standard systems; polyethylene, graphite, diamond, and hexagonal and cubic boron nitride. It is found that the valence band properties are satisfactorily reproduced. For optical spectra a configurational interaction scheme is required.

Key words: SCFLCAO method for solids – Polyethylene – Graphite – Diamond – Boron Nitride.

1. Introduction

There have been a number of extended-Hückel-based band-structure calculations carried through on 3D solids [1–8]. These have yielded results which, in many important respects, appear to be quite reliable qualitatively. It is, however, desirable to carry through self-consistent field calculations of 3D solids so as to, perhaps, approach quantitative results more closely and to generate a better picture of bonding. Since no self-consistent field method can be more than an approximation to the many-body problem, one is faced with the question of which type of self-consistent field method is *adequate* and *practical* for calculation involving solids. The *ab initio* self-consistent field method for solids, which has been applied to linear polymers with reasonable success [9–16], seems desirable

0040–5744/80/0057/0001/$04.60

but is completely impractical at present for real three-dimensional solids containing large atoms and having low symmetry. Hence, one is compelled to fall back on semi-empirical self-consistent field methods. The augmented-plane-wave (APW) self-consistent method used by Neckel et al. [17–19] and the orthogonalised plane-wave method [30] have been shown to be useful for a number of binary materials and, as a complement to this, we have developed an improved semi-empirical method for solid-state calculations based on the tight-binding LCAO approach. Here the interpretation of calculated quantities poses little problem. Hence, we have extended and improved the LCAO CNDO SCF method [21, 22] as formulated for three-dimensional solids by McAloon and Perkins [23].

A number of CNDO SCF calculations for linear polymers, both carbon-only and containing heteroatoms, have already been reported in the literature. A representative sample may be found in Refs. [24–29]. From the results, broad valence- and narrow conduction bands are found, and this is due mainly to the neglect of differential overlap. However, in solids, orbital overlap plays an essential role in determining the crystal eigenvalues: this is particularly true for the 3D case, where high site-symmetry and coordination numbers are the rule. Moreover, because of the nature of the basis Bloch orbitals, the secular determinant has to be solved with the retention of off-diagonal elements of the overlap matrix. We therefore sought a method which, whilst retaining the basic simplicity exhibited by the CNDO method, would take account of overlap and which would predict reasonable valence and conduction-band properties. A recent publication by Harker and Larkins [30] sets out a method similar in many respects to the one we are proposing. They construct and solve the secular determinant for a Large Unit Cell (LUC) micro-crystal using periodic boundary conditions and the CNDO formalism. Results show their method to be effective and efficient for the systems studied. The main difference in approach is that, while they were concerned with the feasibility of LUC methods for solids, we are primarily interested in those modifications which need to be made to CNDO in order that it can be applied to solids with as much reliability as it can at present be applied to molecules. In this Paper we deal with the various problems which are encountered and the modifications made to the CNDO scheme, in order to develop a method which will produce physically reasonable results. Finally, we describe some of the test-band-structures for solids, obtained using this modified technique.

2. Calculational Method

In this section we discuss the problems encountered in extending the CNDO theory of molecules and the modifications made to it, for its application to solids. We consider these under four heads: firstly, we discuss the problem of incorporating into the calculation the non-orthogonal nature of the atomic orbitals; this is required for the calculation of physically realistic eigenvalue spectra of solids. Secondly, in sections (ii) and (iii) we describe the techniques used to approximate the terms involved in the calculation of the two-electron part of the Hamiltonian (i.e. the repulsion integrals and the density matrix elements $P^{0n}_{\lambda\sigma}$) for solids, under

the CNDO framework. Finally, we discuss a new parameter introduced to help calibrate the CNDO results against those obtained by *ab initio* calculations.

2.1. Modification of the Zero-differential-overlap Scheme

The major approximation in the CNDO theory results from the neglect of differential overlap in the construction of the secular determinant. This arises from the assumed orthogonal nature of the atomic orbitals in the CNDO theory. Since the overall sum of orbital overlaps accumulated in overlapping Bloch functions is usually high (because of the large number of neighbours of different rank), the ZDO approximation is a severe one and, hence, we need to develop a method where the non-orthogonal nature of atomic orbitals is, at least partially, recognised. In order to achieve this, we must modify the off-diagonal elements of the interaction matrix. This is most easily seen as follows:

Consider a hydrogen molecule for which the Hamiltonian is $\boldsymbol{H}$. In the usual notation

$$H_{ij} = \langle \phi_i | \boldsymbol{H} | \phi_j \rangle$$

$$S_{ij} = \langle \phi_i | \phi_j \rangle.$$

Orthogonal (*oao*) and non-orthogonal (*ao*) basis sets give rise to the molecular orbital energies, $\varepsilon_{bonding}$ and $\varepsilon_{antibonding}$

$$\varepsilon_{b(oao)} = H_{11} + H_{12}, \qquad \varepsilon_{b(ao)} = \frac{H_{11} + H_{12}}{1 + S_{12}}$$

$$\varepsilon_{a(oao)} = H_{11} - H_{12}, \qquad \varepsilon_{a(ao)} = \frac{H_{11} - H_{12}}{1 - S_{12}}.$$

It is easily shown that application of a constant potential field $\boldsymbol{V}$ will raise the one-electron energy levels of the system by $\boldsymbol{V}$ units of energy. This will apply equally to both orthogonal and non-orthogonal bases but, in order to achieve the result in the latter case, we need to modify the secular determinant thus,

$$\begin{vmatrix} H_{11} + \boldsymbol{V} - \boldsymbol{E} & H_{21} + \boldsymbol{V}\boldsymbol{S}_{21} - \boldsymbol{E}\boldsymbol{S}_{21} \\ H_{12} + \boldsymbol{V}\boldsymbol{S}_{12} - \boldsymbol{E}\boldsymbol{S}_{12} & H_{22} + \boldsymbol{V} - \boldsymbol{E} \end{vmatrix} = 0$$

so that the external applied field only raises or lowers but does not further separate the one-electron energies of the system.

Under the CNDO approximations, as reformulated by Armstrong, Perkins, and Stewart [31], the diagonal and off-diagonal matrix elements of the Hartree–Fock Hamiltonian are given by Eqs. (2.1) and (2.3) as,

$$F_{\lambda\lambda} = -I_{\lambda\lambda} + (1 - \tfrac{1}{2}P_{\lambda\lambda})\gamma_{AA} + \sum_{\sigma} (P_{\sigma\sigma} - P^{g}_{\sigma\sigma})\gamma_{AB} \tag{2.1}$$

$$F_{\lambda\sigma} = -\mathrm{A}S_{\lambda\sigma}(I_{\lambda\lambda}I_{\sigma\sigma})^{1/2} - \tfrac{1}{2}P_{\lambda\sigma}\gamma_{AB}. \tag{2.2}$$

Eq. (2.1) can be rewritten as,

$$F_{\lambda\lambda} = -I_{\lambda\lambda} + (1 - \tfrac{1}{2}P_{\lambda\lambda})\gamma_{AA} + M'_{\lambda\lambda} \tag{2.3}$$

where

$$M'_{\lambda\lambda} = \sum_{\sigma} (P_{\sigma\sigma} - P^{g}_{\sigma\sigma})\gamma_{AB} \tag{2.4}$$

represents the constant potential-energy term arising from elements of the Hartree–Fock Hamiltonian as expressed in Eqs. (2.1) and (2.2) and will show the correct effect of the potential-energy term $M'_{\lambda\lambda}$ on the molecular-orbital energy levels of the system for the orthogonal basis set. However, for this to be true in the non-orthogonal basis set, the off-diagonal matrix elements of the Hartree–Fock Hamiltonian of Eq. (2.2) must be modified as follows,

$$F_{\lambda\sigma} = -\mathrm{A}S_{\lambda\sigma}(I_{\lambda\lambda}I_{\sigma\sigma})^{1/2} - \tfrac{1}{2}P_{\lambda\sigma}\gamma_{AB} + \tfrac{1}{2}S_{\lambda\sigma}(M'_{\lambda\lambda} + M'_{\sigma\sigma}). \tag{2.5}$$

Hence, replacing (2.2) by (2.5) for $F_{\lambda\sigma}$ allows the solution of the secular determinant $|\boldsymbol{H} - \boldsymbol{ES}| = 0$ with the retention of the off-diagonal elements of the overlap matrix.

2.2. Construction of the γ-repulsion integral

The matrix elements arising from the two-electron part of the Hartree–Fock Hamiltonian under the CNDO approximations are evaluated using γ-integrals. For example, the term $M'_{\lambda\lambda}$ in Eq. (2.4) has the following form when applied to periodic solids,

$$M'_{\lambda\lambda} = \sum_{\sigma} (P^{00}_{\sigma\sigma} - P^{00g}_{\sigma\sigma}) \sum_{n=-(N/2)}^{N/2} \gamma^{0n}_{\lambda\sigma} \tag{2.6}$$

$$M'_{\lambda\lambda} = \sum_{\lambda \in A} (P^{00}_{\lambda\lambda} - P^{00g}_{\lambda\lambda})\, \gamma^{00}_{\lambda\lambda} + M_{\lambda\lambda} \tag{2.7}$$

where the 1st term in Eq. (2.7) represents the change in the one-electron energy levels of atom A due to the presence of the charge on Atom A, and the second term, $M_{\lambda\lambda}$, is the Madelung potential energy experienced by an atomic orbital ϕ_λ centred on atom A situated in the central unit cell of the lattice. However, the nature of a solid requires a large number of γ-integrals to be calculated for $M_{\lambda\lambda}$. The correct evaluation of these integrals is, therefore, of some importance. The standard techniques [32] for evaluating γ-integrals give reasonable results for small molecules but when applied to solids can give rise to very significant errors. In order to overcome this difficulty we have developed the following method for the evaluation of γ-integrals which, whilst retaining simplicity, produces the correct behaviour of the Madelung potential-energy term for solids.

The electrostatic repulsion energy $\gamma_{\lambda\sigma}$ between the electrons in the atomic orbitals ϕ_λ and ϕ_σ is

$$\gamma_{\lambda\sigma} = \iint \phi^2_\lambda(1) \frac{1}{r_{12}} \phi^2_\sigma(2)\, d\tau_1\, d\tau_2. \tag{2.8}$$

We seek an approximate method for calculating $\gamma_{\lambda\sigma}$ which avoids numerical integration but, at the same time, will produce physically realistic results. We proceed by first making the following two assumptions:

a. The atomic orbitals can be represented by spheres within which the electron density is uniform and outside which the electron density is zero.

b. The diameter, d_A, in Å, of such a sphere can be approximated by using the electrostatic Coulomb repulsion as,

$$\mathbf{d}_A = \frac{14.397}{\gamma_{\lambda\lambda}}. \tag{2.9}$$

For any two atomic orbitals ϕ_λ and ϕ_σ, $\gamma_{\lambda\sigma}$ can be calculated in the following way.

Let R_A and R_B be the radii of the spheres representing two atomic orbitals, ϕ_λ and ϕ_σ, whose centres are separated by a distance R_{12}. Then R_C, R_D, the radii of the point charge spheres, as shown in Fig. 1, are given by

$$R_C = R_{12} - R_A \tag{2.10}$$

$$R_D = R_{12} - R_B. \tag{2.11}$$

The electron density within the sphere of radius R_C experiences a repulsion due to a point charge at a distance R_{12}. Similarly, the electron density within the sphere of radius R_D is repelled by the electron density of ϕ_λ acting as a point charge at a distance R_{12}. This contributes a term γ_1 to the overall γ-integral, given by

$$\gamma_1 = \left(\frac{R_C}{R_A}\right)^3 \times \frac{C}{R_{12}} = \left(\frac{R_D}{R_B}\right)^3 \times \frac{C}{R_{12}} \tag{2.12}$$

depending upon which centre we base our derivation.

Let us use the centre of ϕ_λ, then

$$\gamma_1 = \left(\frac{R_C}{R_A}\right)^3 \times \frac{C}{R_{12}}$$

where $C = 14.397$.

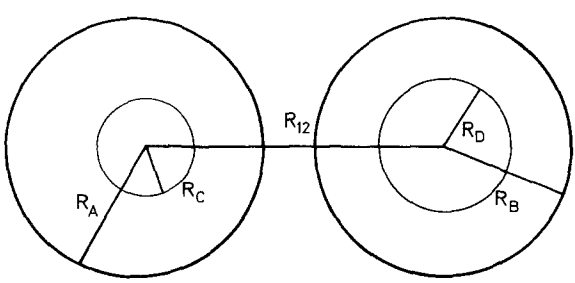

Fig. 1. Geometrical construction for repulsion integrals

The next term, γ_2, is the repulsion of the shell $(R_A - R_C)$ by the core of ϕ_σ, equivalent to the sphere of radius R_D. This can be approximated as,

$$\gamma_2 = \left\{1 - \left(\frac{R_C}{R_A}\right)^3\right\}\left(\frac{R_D}{R_B}\right)^3 \times \frac{C}{R_{12}} \tag{2.13}$$

$$= \left\{\left(\frac{R_D}{R_B}\right)^3 - \left(\frac{R_C R_D}{R_A R_B}\right)^3\right\} \times \frac{C}{R_{12}}. \tag{2.14}$$

The third remaining term, γ_3, is the repulsion of the shell $(R_A - R_C)$ by $(R_B - R_D)$. This can be approximated by an expression similar to Mataga's [32], i.e.

$$\gamma_3 = \left(\frac{C^2}{\gamma_<^2} + R_{12}^2\right)^{-1/2}\left\{\left(1 - \left[\frac{R_C}{R_A}\right]^3\right)\left(1 - \left[\frac{R_D}{R_B}\right]^3\right)\right\} \times C \tag{2.15}$$

where $\gamma_<$ is the lesser of the two γ-values.

Finally, the full γ-integral arising from the repulsion between two electrons in the atomic orbitals ϕ_λ and ϕ_σ separated by a distance R_{12} is given by the sum of these three terms as,

$$\gamma_{\lambda\sigma} = \left\{\left(\frac{R_C}{R_A}\right)^3 + \left(\frac{R_D}{R_B}\right)^3 - \left(\frac{R_D R_C}{R_A R_B}\right)^3\right\} \times \frac{C}{R_{12}}$$
$$+ \left(\frac{C^2}{\gamma_<^2} + R_{12}^2\right)^{-1/2} \times \left\{\left[1 - \left(\frac{R_C}{R_A}\right)^3\right]\left[1 - \left(\frac{R_D}{R_B}\right)^3\right]\right\}. \tag{2.16}$$

For limiting values of R_{12}, the above equation has the following values,

$$R_{12} = 0; \quad R_c = 0; \quad R_D = 0; \quad \gamma_{\lambda\sigma} = \gamma_<$$

$$R_{12} > R_A + R_B; \quad R_C = R_A; \quad R_D = R_B; \quad \gamma_{\lambda\sigma} = \frac{C}{R_{12}} \tag{2.17}$$

$$R_A + R_B > R_{12} > R_A; \quad \gamma_< < \gamma_{\lambda\sigma} < \frac{C}{R_{12}}$$

which are in line with physical intuition.

Evaluation of $\gamma_{\lambda\sigma}$ using Eq. (2.17) affords the correct behaviour of the Madelung term in ionic solids. Hence, in all our calculations we have used this new technique for evaluating the γ-integrals.

2.3. Construction of the Density Matrix $\boldsymbol{P}$ *for Crystals*

The density and bond-order matrix $\boldsymbol{P}$ for solids is constructed from the set of molecular-orbital coefficients $\boldsymbol{C}_{\lambda j}(\boldsymbol{k})$ as described in Eq. (2.16), *viz.* the elements are,

$$P_{\lambda\sigma}^{0n} = O_j \sum_{\boldsymbol{K}} \sum_{\substack{\text{all } j \\ \text{occ}}} \mathbf{C}_{\lambda j}^*(\boldsymbol{k}) \mathbf{C}_{\sigma j}(\boldsymbol{k}) \exp(i\boldsymbol{k} \cdot \boldsymbol{R}n) \tag{2.18}$$

For the correct behaviour of $P^{0n}_{\lambda\sigma}$, the sum over $\boldsymbol{k}$ should be carried out over the first Brillouin zone of the system in a continuous fashion. This can be achieved by constructing a commensurate mesh of $\boldsymbol{k}$-points in the first Brillouin zone, which then can be taken for the sum over $\boldsymbol{k}$-points in Eq. (2.16). This technique, although simplifying the problem to some extent, does not reduce it: one still has to construct and diagonalise the secular determinants for each value of $\boldsymbol{k}$ in order to obtain the coefficients, $\mathbf{C}_{\mu p}(\boldsymbol{k})$. We simplify this massive problem through the crystal symmetry.

Now, all the distinct crystal orbitals can be obtained by diagonalising secular determinants each corresponding to a value of the wave vector lying within or on the surface of the representation domain of the Brillouin zone. Moreover, the wave vector $\boldsymbol{k}$ out of which the star is generated can always be chosen to lie on or within the surface of this representation domain.

We therefore exploit the symmetry properties of the wave vector and the space group operations $\{\hat{\boldsymbol{R}}_\alpha|\hat{\omega}_\alpha\}$ of the crystal to obtain the density matrix for the crystal. The procedure used is illustrated in the flow diagram shown in Fig. 2. This procedure reduces to an irreducible minimum the number of constructions and diagonalisations of the secular determinants required for a given number of $\boldsymbol{k}$-points, i.e., to the number of $\boldsymbol{k}$-points lying in the representation domain. However, in order to obtain the correct size of mesh of $\boldsymbol{k}$-points required for the final density matrix $\boldsymbol{P}$ of the crystal, we use the following property of the matrix.

Given an orthonormal set of non-back-transformed eigenvectors, the density matrix $\boldsymbol{P}$ constructed using these coefficients is duodem-potent, i.e.

$$\boldsymbol{P}^2 = 2\boldsymbol{P}. \tag{2.19}$$

As the eigenvectors of a crystal are orthonormal, we have,

$$2P^{00}_{\lambda\lambda} = \sum_{n=-N/2}^{N/2} \sum_{\sigma} \{P^{0n}_{\lambda\sigma}\}^2. \tag{2.20}$$

Eq. (2.19) is satisfied only when the $\boldsymbol{k}$-points used in Eq. (2.18) are equal in number to $\boldsymbol{N}$, the number of unit cells considered in the lattice, and their positions in reciprocal space are determined in a definite way by the unit-cell positions in real space. We introduce an error function $\mathrm{P_E}$ to monitor the correct mesh type and size required for the construction of the density matrix, $\boldsymbol{P}$ which satisfies the space-group symmetry of the lattice as follows:

$$P_e(\lambda) = 2P^{00}_{\lambda\lambda} - \sum_{n=-N/2}^{N/2} \sum_{\sigma} \{P^{0n}_{\lambda\sigma}\}^2 \tag{2.21}$$

and

$$\mathrm{P_E} = \sum_{\lambda=1}^{m} P_e(\lambda). \tag{2.22}$$

For a correct mesh the function $\mathrm{P_E}$ will vanish. In practice we observe the behaviour of $\mathrm{P_E}$ whilst varying the mesh size and type until $\mathrm{P_E}$ is acceptably close

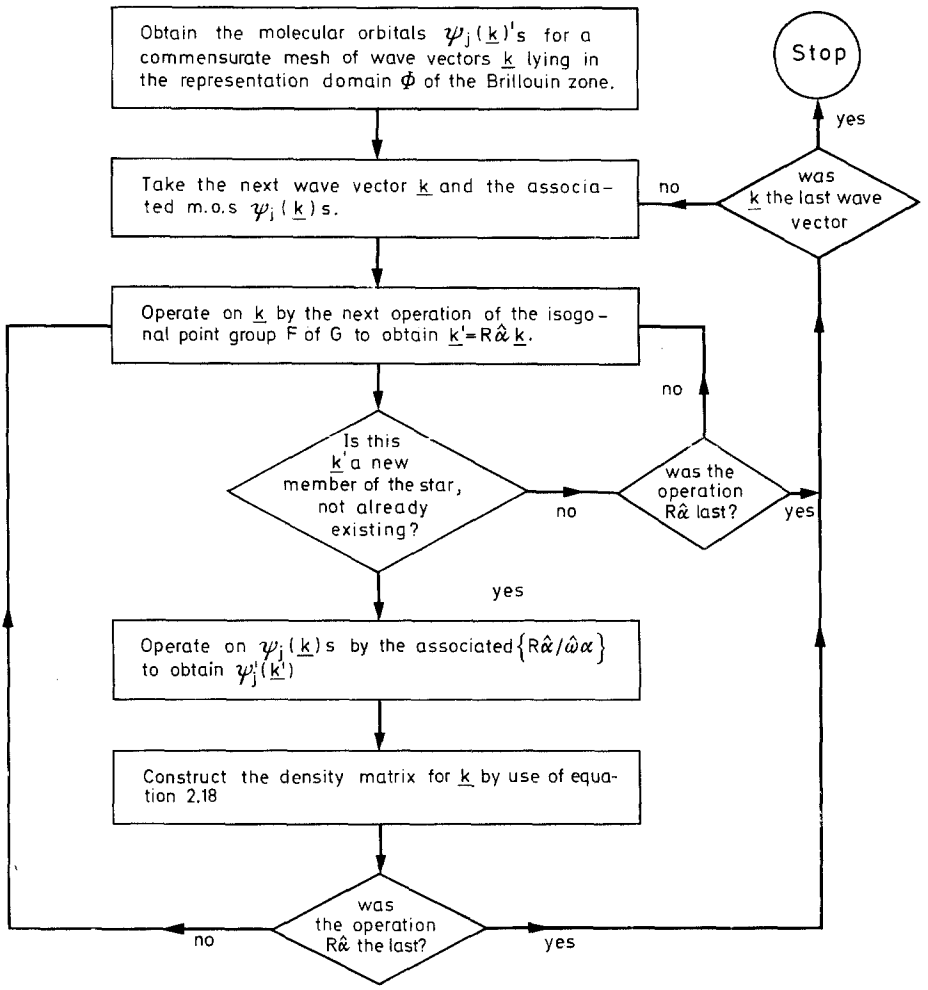

Fig. 2. Flow diagram for construction of the density matrix

to zero. This provides us with a method for determining an adequate crystal density matrix for the self-consistent-field calculations.

2.4. Modification of the Overlap Matrix

The complex nature of the energy bands and associated properties of crystals puts very considerable stress on any method used for their calculation. This is particularly striking when one considers the large number of "types" of solids which one is trying, calculationally, to describe. As aforementioned, however, for a limited class of materials, the simple linear carbon-based polymers, calculations of varying complexity have been carried through, including *ab initio* methods [9–16, 24–30]. These latter have been effected with Gaussian-based orbitals essentially

equivalent to the basis sets currently popular and successful in quantum chemical calculations for molecules. It seems at present that this type of approach is the best that can be achieved, the calculations being generally consistent one to the other (which is not always true of experimental results). Hence, in choosing a touchstone against which to measure and match the semi-empirical approach, we have chosen these *ab initio* results.

Previous semi-empirical calculations on polymers have assumed zero differential overlap. Here we have formulated the theory without this condition. We can, however, investigate the intermediate situations lying between the two extremes by inclusion of an overlap weighting parameter α. Hence, α is used to modify elements of the overlap matrix $\boldsymbol{S}$ required for the construction of the secular determinant. Thus, we have

$$|F_{\lambda\sigma} - \varepsilon_i S'_{\lambda\sigma}| = 0 \tag{2.23}$$

where

$$S'_{\lambda\sigma} = S_{\lambda\sigma}(\delta_{\lambda\sigma} + \alpha(1 - \delta_{\lambda\sigma})). \tag{2.24}$$

The extreme values of this α parameter have already been used in the construction of the secular determinant of equation (i.e. $\alpha = 1$ in the *ab initio* and $\alpha = 0$ in the CNDO methods). We find (*vide infra*) that it allows us to parametrise band structures satisfactorily close to those obtained by the *ab initio* methods. We further describe this parametrisation procedure in Sect. 3.

2.5. Matrix Elements of the Hamiltonian and the Overlap Matrices under the Modified CNDO Theory of Solids

The matrix elements of the Hamiltonian and the overlap matrices, using the above proposed modifications to the CNDO theory, are,

$$F_{\lambda\lambda}(\boldsymbol{k}) = -I_{\lambda\lambda} + (1 - \tfrac{1}{2}P^{00}_{\lambda\lambda})\gamma^{00}_{\lambda\lambda} + M'_{\lambda\lambda} - \sum_{n=-N/2}^{N/2} \cos \boldsymbol{k} \cdot \boldsymbol{R}_n [\boldsymbol{A} I_{\lambda\lambda} S^{0n}_{\lambda\lambda} + \tfrac{1}{2}P^{0n}_{\lambda\lambda}\gamma^{0n}_{\lambda\lambda} - S'^{0n}_{\lambda\lambda} M'_{\lambda\lambda}] \tag{2.25}$$

$$F_{\lambda\sigma}(\boldsymbol{k}) = -\sum_{n=-N/2}^{N/2} \exp(i\boldsymbol{k} \cdot \boldsymbol{R}_n)[\boldsymbol{A} S^{0n}_{\lambda\sigma}(I_{\lambda\lambda} I_{\sigma\sigma})^{1/2} + \tfrac{1}{2}P^{0n}_{\lambda\sigma}\gamma^{0n}_{\lambda\sigma}] + \tfrac{1}{2}\sum_{n=-N/2}^{N/2} S^{0n}_{\lambda\sigma}(M'_{\lambda\lambda} + M'_{\sigma\sigma}) \exp(i\boldsymbol{k} \cdot \boldsymbol{R}_n) \tag{2.26}$$

where

$$M'_{\lambda\lambda} = \sum_{\sigma} (P^{00}_{\sigma\sigma} - P^{oog}_{\sigma\sigma}) \sum_{n=-N/2}^{N/2} \gamma^{0n}_{\lambda\sigma}$$

$$S'_{\lambda\lambda}(\boldsymbol{k}) = 1 + \sum_{n=-N/2}^{N/2} \alpha \cos(\boldsymbol{k} \cdot \boldsymbol{R}_n) S^{0n}_{\lambda\lambda}$$

$$S'_{\lambda\sigma}(\boldsymbol{k}) = \sum_{n=-N/2}^{N/2} \alpha \exp(i\boldsymbol{k} \cdot \boldsymbol{R}_n) S^{0n}_{\lambda\sigma}.$$

The secular determinants have the form,

$$|F_{\lambda\sigma}(\boldsymbol{k}) - \varepsilon_j(\boldsymbol{k}) S'_{\lambda\sigma}(\boldsymbol{k})| = 0.$$

3. Results and Discussion

In this section we describe the calibration and testband structures for some simple solids found using the present method. This serves, firstly, as an investigation into the capability of the method to calculate the complex energy bands in solids and, secondly, to give us some insight into the behaviour of the Mulliken–Wolfsberg–Helmholtz and the overlap parameters, **A** and α, respectively. Finally, the calculations provide a test of the error function, P_E, used to monitor the adequacy of the density matrix required for the self-consistent calculations of solids.

3.1. Polyethylene

A good starting example is that of polyethylene, for which *ab initio* band structures exist. We parametrised the present semi-empirical band structure of polyethylene against the most recent *ab initio* results of Armstrong et al. [15]. The material is treated as a one-dimensional linear polymer with lattice parameter $a = 2.51688$ Å. We took into account the interactions between seven unit cells of the polymer (i.e. up to sixth-nearest neighbours).

The orbital exponents and the valence-state ionisation potentials used are given in Table 1. The valence orbital ionisation potentials used in this work were abstracted from the work of Levison and Perkins [53], who calculated these from spectral data. Burn's Rules were employed for the calculation of most of the orbital exponents used in this work except for C, B, and N, where the orbital exponents used were as for the *ab initio* work of Armstrong et al. [15]. The one-centre two-electron repulsion integrals, γ_{AA}, used in this work were calculated using the Eq. (2.16). The effect of the mesh size and the variable parameters, MWH constant A and the overlap parameter, α, was studied as follows:

3.2. Variation in Commensurate Mesh Size

As described in Sect. 2, we use the error function P_E to find the mesh of $\boldsymbol{k}$-points which gives an adequate density matrix required for the self-consistent cal-

Table 1. Atomic input data

	Orbital exponent		Valence orbital ionisation potential $I_{\lambda\lambda}$(eV)		Two-electron one-centre integrals γ_{AA}(eV)
	s	*p*	*s*	*p*	
H	1.0	—	13.06	—	12.84
B	1.288	1.21	14.05	8.30	12.84
C	1.608	1.568	19.44	10.67	10.01
N	1.923	1.917	25.58	13.19	14.81

Table 2. Relation between P_E and the mesh sizes for polyethylene

No. of k-points in range $0-\pi/a$	P_E
1	−287.9
2	−126.4
3	−40.3
4	−10.2
5	10^{-4}
6	10^{-6}
7	10^{-6}
12	10^{-6}

culation. The one-dimensional first Brillouin zone for polyethylene has range

$$\mathcal{O}(\Gamma) < \boldsymbol{k} < \pm\frac{\pi}{a}(X).$$

The correct density matrix $\boldsymbol{P}$ is obtained by summing over the wave vectors in Eq. (2.18) extending over the entire Brillouin zone. However, we can exploit the time-reversal symmetry of Brillouin zones in order to cut down the number of constructions and diagonalisations of the secular determinants. This is because $\psi(\boldsymbol{k})$ and $\psi^*(\boldsymbol{k})$ give rise to equivalent density matrices and so we can use the wave vectors lying in half of the first Brillouin zone to construct the density matrix for the system. Thus, in one-dimensional periodic solids, we can use the wave vectors lying in the range $(0-\pi/a)$ to construct the density matrix.

Table 2 shows the relationship between P_E and the mesh sizes used for test calculations of polyethylene with MWH constant A = 1.4 and overlap parameter $\alpha = 0.80$ (*vide infra*). Examination of Table 2 reveals that six equidistant $\boldsymbol{k}$-points in the reduced part of the first Brillouin zone affords a good density matrix for polyethylene.

3.3. Variation of the MWH Constant, A, and the Overlap Parameter, α

Fig. 3 shows the effect of varying A and α on the band structure of polyethylene calculated using six points in the irreducible part of the Brillouin zone. Examination of Fig. 3 reveals the following two generalisations, firstly, the band gap and the band width increase with increasing value of A and, secondly, the band gap decreases and the band width increases with decreasing value of α.

Values of 1.4 and 0.60 for the MWH constant A and the overlap parameter α, respectively, produce a band structure visually closest to the *ab initio* results.

Finally, Fig. 4 shows the self-consistent band structure of polyethylene calculated using the above-obtained values of 1.4 and 0.60 for A and α, respectively, superimposed on the *ab initio* results of Armstrong et al. [15]. The calculated ionisation potential of 9.07 eV is in acceptable agreement with the *ab initio* result

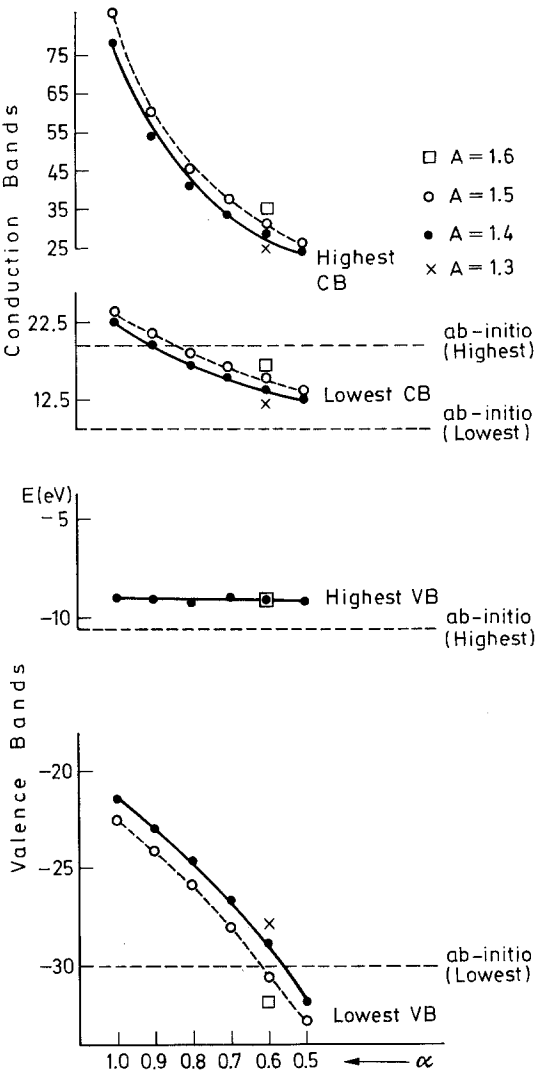

Fig. 3. Effect of the variable parameters A and α on the band structure of polyethylene

of 10.7 eV (expt. 8.5 eV [33]), whilst the computed charges of $C^{-0.24}$ and $H^{+0.12}$ are comparable with the *ab initio* values of $C^{-0.36}$ and $H^{+0.18}$.

3.4. Two-dimensional Graphite

Next, we describe self-consistent band-structure calculations for two-dimensional graphite using the above-obtained values of A and α. In the two-dimensional graphite structure, there are two atoms per unit cell. The primitive translation vectors are $t_a = t_b = 2.45085$ Å, optimised by Dovesi *et al.* [34]. The first Brillouin zone is a hexagon and is shown in Fig. 5 along with the notation of Lomer [35] for the symmetry points.

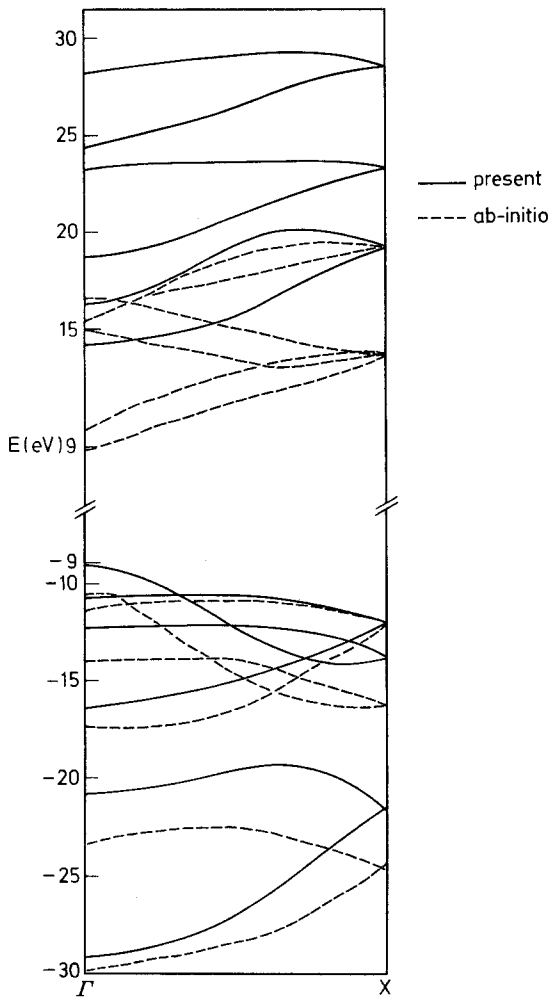

Fig. 4. SCF band structure of polyethylene superimposed on *ab initio* results (Ref. 15)

Unit cells lying within the circle of radius 8 Å were considered as interacting with the central unit cell. The representation domain Φ and the basic domain Ω both have volumes equal to one-twelfth that of the first Brillouin zone. The different commensurate meshes are shown in Fig. 6, with the $\boldsymbol{k}$-points lying in the basic domain, and Tables 3–5 give their positions in terms of ($\boldsymbol{b}_1$, $\boldsymbol{b}_2$), the vectors of the reciprocal space.

Table 6 gives the total number of $\boldsymbol{k}$-points generated in the Brillouin zone using these meshes in the basic domain Ω. Finally, Table 7 shows the relationship between the error function, P_E, and the mesh sizes. The band structure of graphite does not show any variation on increasing the number of sampling points in the basic domain from 19 to 25. This implies that mesh 4 gives a good density matrix.

Fig. 7 shows the self-consistent band structure for graphite, calculated using 25 sampling points in the basic domain Ω. Table 8 shows the various features of the

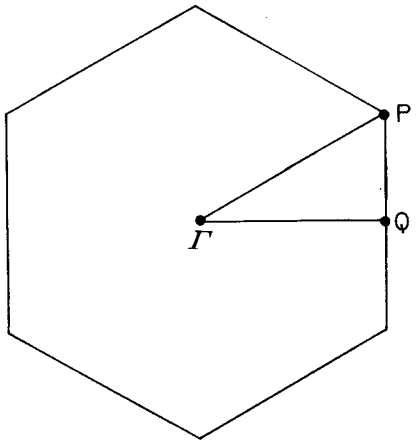

Fig. 5. Brillouin zone for 2D graphite

valence band as obtained in the present work, along with the results of first-principle calculations of Painter and Ellis [36] and those of Corbato [37]. Our calculated value of the total valence-band width of 29.0 eV is also in line with the recent experimental value of 24.1 eV obtained by McFeely et al. [38].

The Fermi level calculated in the present work at -4.52 eV is in good accord with the experimental value of -4.60 eV also determined by McFeely [38]. We would expect that the results of our calculations would be improved with respect to the experimental values if the calculations brought in the third dimension of graphite. This is because the third dimension of the crystal splits the degeneracy at the ***P*** point and both the Fermi level and the total band width are lowered. It should be

Table 3. Positions of k-points in Ω corresponding to Mesh 1 (Fig. 5)

k-point	Position b_1	b_2
1	0	0
2	$6a$	0
3	$4a$	$2a$
4	$8a$	$4a$

Table 4. Positions of k-points in Ω corresponding to Mesh 2 (Fig. 5)

k-point	Position b_1	b_2	k-point	Position b_1	b_2
			5	$5a$	a
1	0	0	6	$4a$	$2a$
2	$3a$	0	7	$7a$	$2a$
3	$6a$	0	8	$6a$	$3a$
4	$2a$	0	9	$8a$	$4a$

Table 5. k-point positions in Ω corresponding to meshes 3 and 4 (Fig. 5)

Mesh 3 ($a = b_{1/12} = b_{2/12}$)			Mesh 4 ($c = b_{1/24} = b_{2/24}$)		
	Position			Position	
k-point	b_1	b_2	k-point	b_1	b_2
1	0	0	1	0	0
2	a	0	2	$3c$	0
3	$2a$	0	3	$6c$	0
4	$3a$	0	4	$9c$	0
5	$4a$	0	5	$12c$	0
6	$5a$	0	6	$2c$	c
7	$6a$	0	7	$5c$	c
8	$2a$	a	8	$8c$	c
8	$3a$	a	9	$11c$	c
10	$4a$	a	10	$4c$	$2c$
11	$5a$	a	11	$7c$	$2c$
12	$6a$	a	12	$10c$	$2c$
12	$4a$	$2a$	13	$13c$	$2c$
14	$5a$	$2a$	14	$6c$	$3c$
15	$6a$	$2a$	15	$9c$	$3c$
16	$6a$	$2a$	16	$12c$	$3c$
17	$6a$	$3a$	17	$8c$	$4c$
18	$7a$	$3a$	18	$11c$	$4c$
19	$8a$	$4a$	19	$14c$	$4c$
			20	$10c$	$5c$
			21	$13c$	$5c$
			22	$12c$	$6c$
			23	$15c$	$6c$
			24	$14c$	$7c$
			25	$16c$	$8c$

pointed out here that our calculation is in no way adjusted to *fit* the band structure of graphite but involves only a transfer of two parameters from polyethylene. Moreover, the results obtained are a significant improvement over the conventional CNDO results of Dovesi et al. [34], where the valence band width

Table 6. Relation between the number of k-points in Ω and the number of generated k-points in the F.B.Z. of graphite

Mesh	No. of k-points in Ω	Total no. of k-points in B.Z.
1	4	12
2	9	48
3	19	144
4	25	192

Table 7. Relation between mesh sizes and PE

Mesh	Mesh 1	Mesh 2	Mesh 3	Mesh 4
P_E	−142.24	0.08	10^{-4}	10^{-6}

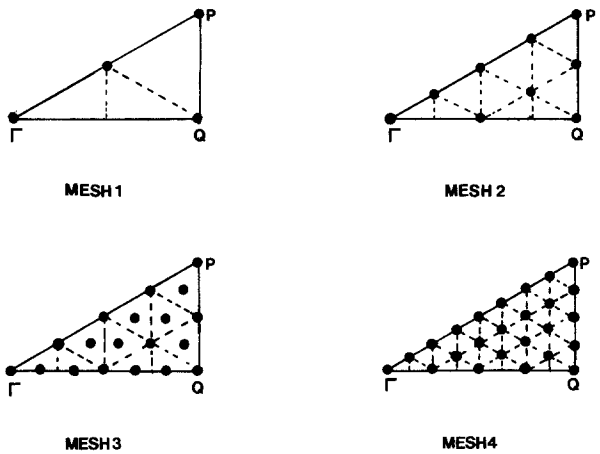

Fig. 6. Commensurate meshes for the 2D-hexagonal lattice (in the representation zone)

obtained is three times the experimental value. The charge distribution within the valence orbitals corresponds essentially to the "sp^2" configuration usually quoted for trigonal carbon atoms in planar organic compounds.

3.5. Two-dimensional Boron Nitride

Hexagonal boron nitride is isoelectronic with graphite and a two-dimensional sheet has a primitive unit cell containing one atom of boron and one atom of nitrogen. We took the unit cell to have B–N bond length 1.45 Å as observed in the

Table 8. Partial valence band widths (W_π and W_σ), the total valence band width (W_{tot}), and σ-π band overlap (Δ_σ) obtained from various calculations. Energy given in eV

Property	Present work	Painter and Ellis*	Corbato†
W_p	12.6	8.0	9.8
W_σ	23.4	16.0	16.6
W_{tot}	29.0	20.8	18.5
$\Delta_{\sigma\text{-}\pi}$	8.0	3.0	6.0

*Ref. [36] †Ref. [37]

Table 9. The total valence band width (W_{tot}) and the band gap obtained from the various calculations. Energy in eV

Property	Present work	Zunger*et al.	Zupan**	Nakhmanson†
W_{tot}	22.75	17.3	16.0	27.8
Band gap	9.1	5.1	4.9	3.6

* Ref. [40] ** Ref. [54] † Ref. [55]

three-dimensional hexagonal structure [39]. Unit cells lying within the sphere of radius 8 Å were allowed to interact with the central unit cell. The valence-state ionisation potentials and orbital exponents used in the calculation are given in Table 1. We have used the values of the variable parameters, A and α, as obtained from the results of the polyethylene calculation. The similar hexagonal structure of graphite and boron nitride allow us to use mesh 4 as used in the former case. The corresponding value of the errror function, P_E, is $\sim 10^{-5}$.

Fig. 8 shows the self-consistent band structure of two-dimensional boron nitride, obtained using the above-described parameters. Table 9 lists the valence band widths and the lowest inter-band transition as obtained in the present work, along with the results of previous calculations.

The present value of the total valence band width (22.7 eV) is compatible with results of X-ray spectra, which indicate a total valence band width of about 18.6 eV. The present value of the band gap at 9.1 eV is larger than the observed optical-absorption edge at 5.8 eV [40]. In a covalent and fairly localised system like a B–N compound, we expect that the experimental optical absorption will not correlate directly with the band gap as it would in a strongly delocalised system. Thus, it is significant that the corresponding eigenvalue difference in borazine amounts to 14.6 eV [41] whereas, after correction by configuration interaction, several states are found, falling in the region 6.6 to 7.5 eV, in good agreement with the observed electronic spectrum [42]. Thus, we expect that the many-electron effects are quite important in the optically exited state of the hexagonal BN crystal (although, because of its less localised nature, not so marked as in borazine itself) and consideration of the configuration interaction between band-to-band excited configurations will bring the 'state band gap' more into line with experiment.

Finally, Table 10 shows the valence orbital charge distribution in boron-nitride along with the related systems borazine and polyboronimide, obtained using the same set of atomic input parameters. Examination of Table 10 reveals that the $2p_\pi$ orbital population for boron and nitrogen atoms tends to unity as we go from polyboronimide to hexagonal boron nitride. This implies an increase in the π-bonding ability of the boron and nitrogen atoms and, thereby, an increase in the π-delocalisation as we go from polyboronimide to hexagonal boron nitride. It is noticeable that the hydrogen atoms of the latter two systems exert a cogent influence on the boron charge population, rendering the atom virtually neutral.

Table 10. Charge distribution in 2D-hexagonal boron nitride and related systems

	Boron			Nitrogen			H(B)	H(N)	Charge	
	$2s$	$2p_\sigma$	$2p_\pi$	$2s$	$2p_\sigma$	$2p_\pi o$	$1s$	$1s$	B	N
Boron nitride	0.80	1.32	0.69	1.17	2.71	1.31	—	—	+0.19	−0.19
Borazine	0.84	1.51	0.61	1.15	2.63	1.39	1.04	0.83	+0.04	−0.17
Poly-boronimide	0.86	1.51	0.55	1.16	2.60	1.45	1.02	0.85	+0.08	−0.21

3.6. *Diamond*

Diamond has the face-centred cubic structure with space group $\mathcal{O}_h^9$. It has two atoms per primitive unit cell stemming from the two interpenetrating face-centred cubic lattices. The lattice parameter is 3.577 Å [43]. The first Brillouin zone for the face-centred cubic lattice is shown in Fig. 9. Interactions between the unit cells lying within a sphere of radius 10 Å were taken into account. All the input data, including α and A, were the same as for polyethylene. Fig. 10 shows the commensurate mesh of 19 $\boldsymbol{k}$-points lying in the basic domain taken for the construction of the density matrix. These 19 points in the basic domain result in 256 points in the first Brillouin zone and in an error function, P_E, $\sim 10^{-6}$.

Fig. 11 shows the self-consistent band structure calculated for diamond. There is a general agreement between our results and the valence band structure calculated by Painter et al. [44] using *ab initio* techniques. Furthermore, the calculated value of the valency band width of ~24.0 eV is in excellent agreement with the experimental value of 24.1 eV obtained by McFeely [38]. The only well-established transition in diamond seems to be that associated with the indirect gap: this amounts to 5.47 eV [45]. The indirect gap is found between the zone centre and a conduction-band minimum at $\boldsymbol{k}_x = 0.39$; $\boldsymbol{k}_y = 0$; $\boldsymbol{k}_z = 0$. Our calculations give the energy of the lowest electronic transition as 11.6 eV. This is direct and involves the Γ_{15} and Γ'_{25} states at the zone centre. Our results are very similar to those produced by the non-self-consistent treatment of Pugh [46], who also obtained a direct interband transition between Γ_{15} and Γ'_{25} states with energy

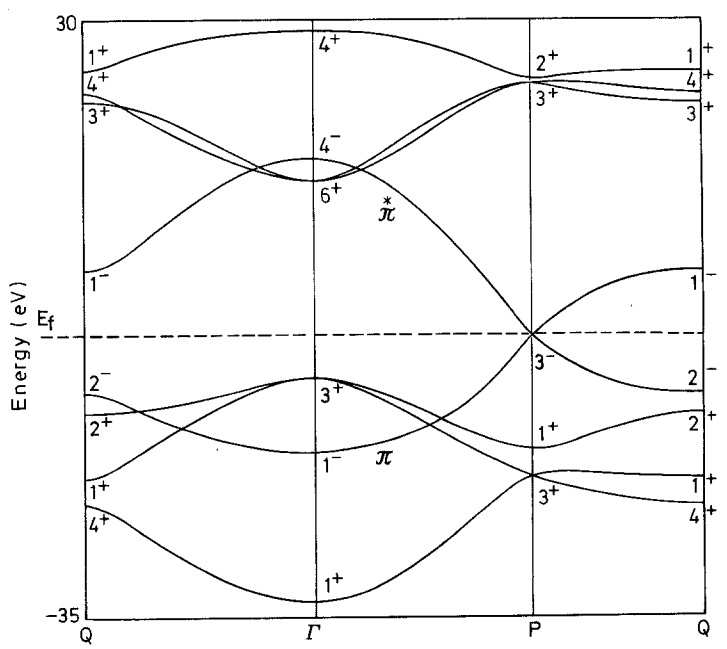

Fig. 7. SCF band structure for graphite

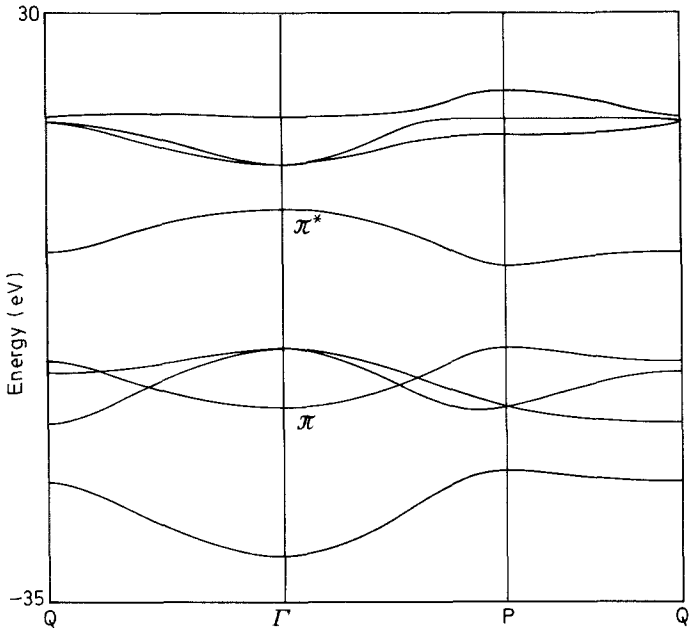

Fig. 8. SCF band structure for hexagonal boron nitride

12.6 eV. It is notable that significant contributions from the carbon $3s$ and $3p$ orbitals to the conduction band were found by Painter et al. [44] and these bases caused the conduction-band minimum to lie along the symmetry line Δ, consistent with the experimental results. We believe our basis set to be deficient to describe the conduction bands though adequate for the valence bands of diamond. We expect that the inclusion of these high-energy carbon orbitals in our calculation would modify the conduction band in the appropriate way. Furthermore, configuration interaction between the band-to-band excited configuration should afford a value of the band gap closer to the experimental findings. Finally, it is interesting that the valence orbital charge distribution, calculated from the valence band, shows "hybridisation" for the carbon atom as, essentially, $2s^1 2p^3$,

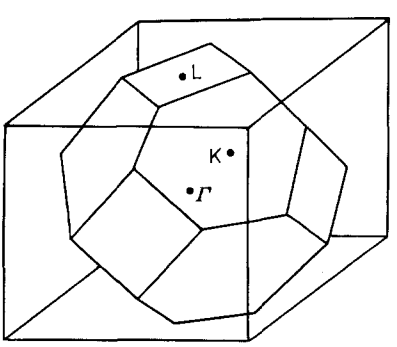

Fig. 9. Brillouin zone for the face-centred cubic lattice

corresponding to the generally assumed "sp^3 hybridisation" in tetrahedral carbon systems.

3.7 Cubic Boron Nitride

Cubic boron nitride has the sphalerite structure with the space group $\mathcal{T}_d^2$. We took the face-centred cubic lattice constant as 3.615 Å [47]. The first Brillouin zone is the same as that of diamond (Fig. 9). All parameters were as used in the hexagonal boron nitride calculation. Nineteen points in the basic domain Ω, giving rise to a total of 256 $\boldsymbol{k}$-points in the first Brillouin zone, were taken for the construction of the density matrix and the resulting value of P_E is $\sim 10^{-5}$.

The calculated energy band structure for cubic boron nitride is shown in Fig. 12, where the maximum of the valence band occurs at Γ, while the conduction-band minimum occurs along the symmetry line from Γ to **X**, with an energy 16.5 eV above the maximum of the valence band. A comparison of the calculated and

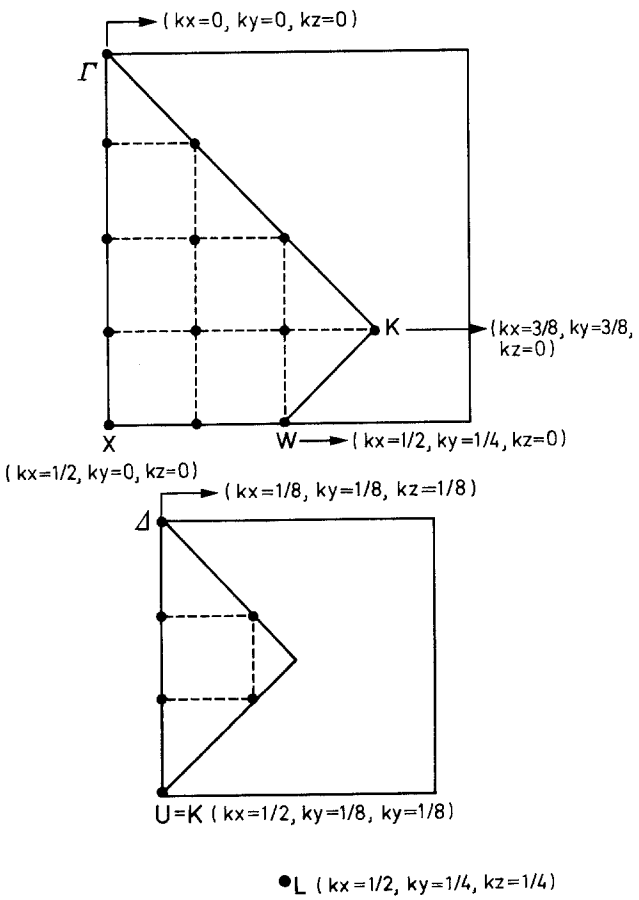

Fig. 10. Commensurate mesh of 19 $\boldsymbol{k}$-points in the representation domain for the FCC lattice

Table 11. Comparison of the calculated and experimental energy band gaps and the valence band widths for cubic boron nitride. Energy in eV

Property	Exptl.††	Bassani and Yoshimine*	Hemstreet† and Fung	Present Work
Direct gap		7.6	8.36	16.73
Indirect band gap	6.0±0.05	2.9	7.6	16.53
Valence band width	15.4±0.5	23.5	27.5	26.28

†† Ref. [48] * Ref. [49] † Ref. [50]

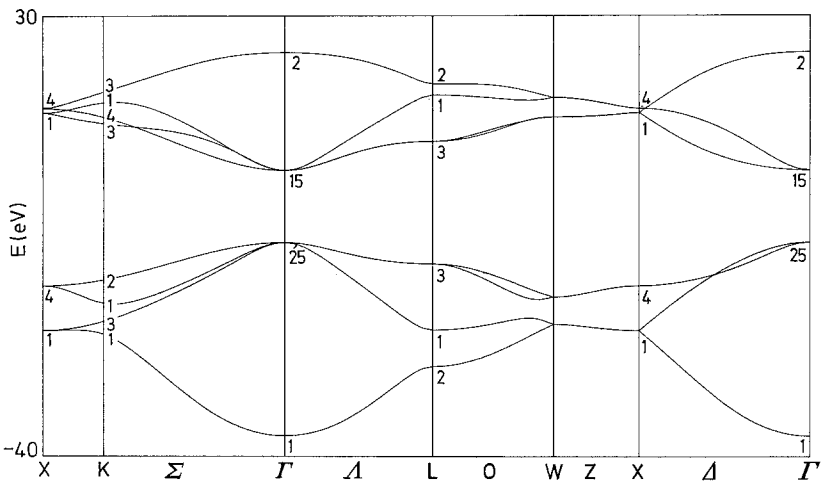

Fig. 11. SCF band structure for diamond

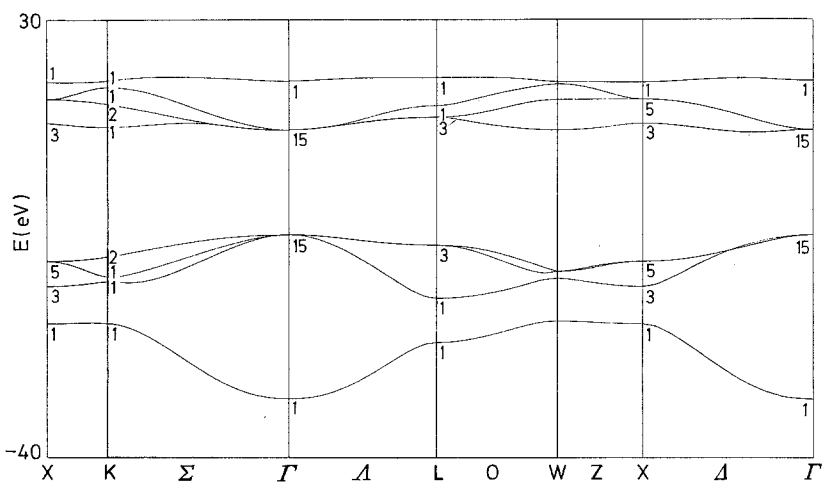

Fig. 12. SCF band structure for cubic boron nitride

experimental energy band gaps and the valence band widths are shown in Table 11.

Our calculated valence band width of 26.28 eV is consistent with the results of previous calculations, although all appear to overestimate this quantity. The lowest interband transition, 16.53 eV, is much higher than the observed absorption-edge energy and, as stated earlier, we expect this to be reduced very substantially by a superimposed C.I. treatment. It is worth noting, however, that this energy lies in the same range as those for the analogous molecules $H_2N\text{-}BH_2$ and $H_3N\text{-}BH_3$ in which the boron atom is also formally 3- and 4-coordinate respectively. Here the eigenvalue gaps are 16.94 eV and 16.87 eV, respectively [51, 52].

Finally, the valence-orbital population calculated from the valence-band results as $B(2s^{0.78}2p^{1.87})$ and $N(2s^{1.19}2p^{4.16})$ (i.e. $B^{+0.35}N^{-0.35}$), thereby emphasising the covalent nature of the material. This is again, basically, what is found for the molecular analogues (Table 11) [50, 51].

4. Conclusion

The semi-empirical self-consistent tight-binding method developed in this work is shown to produce reasonable results for the valence band structures of the solids studied. This allows us to apply it with some confidence to situations where an easily understandable picture of the chemical bonding in the unit cell is desired. Furthermore, our semi-empirical self-consistent method does not involve any more computation than other semi-empirical methods, such as the APW and the pseudo-potential methods but we believe it gives a more easily assimilable interpretation of the chemical bonding in solids. The band gaps do not reproduce observed experimental values for the optical edges but, firstly, the representation of the conduction band can be improved by the inclusion of the virtual orbitals in the basis set used for the band-structure calculations and, secondly, the calculation of optical spectra can be better obtained by superimposing, where relevant, a configuration interaction scheme for the exciton-type states.

Acknowledgement. One of us (AKM) thanks the University of Strathclyde for a Bursary.

References

1. Yamazaki, M.: J. Phys. Soc. (Japan) **12**, 1 (1957)
2. Perkins, P. G., Winter, D. M.: Rev. Roum. Chim. **24**, 285 (1980)
3. Breeze, A.: Solid State Comm. **14**, 395 (1974)
4. Armstrong, D. R., Breeze, A., Perkins, P. G.: J. Chem. Soc. (Faraday II Trans.) **73**, 952 (1976)
5. Breeze, A., Perkins, P. G.: J. Phys. C., Solid State Phys. **5**, 255 (1975)
6. Armstrong, D. R., Perkins, P. G.: J. Chem. Soc. (Faraday II Trans.) **75**, 12 (1979)
7. Breeze, A., Perkins, P. G.: Solid State Comm. **13**, 1031 (1973)
8. Perkins, P. G., Armstrong, D. R., Breeze, A.: J. Phys. C., Solid State Phys. **8**, 3558 (1975)
9. André, J. M., Leroy, G.: Theoret. Chim. Acta (Berl.) **9**, 123 (1967)

10. Karpfen, A., Petkov, J.: Solid State Commun. **29**, 251 (1979)
11. Armstrong, D. R., Jamieson, J., Perkins, P. G.: Theoret. Chim. Acta (Berl.) **51**, 163 (1979)
12. Karpfen, A., Petkov, J.: Theoret. Chim. Acta (Berl.) in Press
13. Kertesz, M., Koller, J., Azman, A.: J. Chem. Phys. **67**, 1180 (1977)
14. Armstrong, D. R., Jamieson, J., Perkins, P. G.: Theoret. Chim. Acta (Berl.) **50**, 193 (1978)
15. Armstrong, D. R., Jamieson, J., Perkins, P. G.: Theoret. Chim. Acta (Berl.) **49**, 55 (1978)
16. Karpfen, A., Chem. Phys. Letters **64**, 299 (1979)
17. Neckel, A., Schwarz, K., Eibler, R., Rastl, P., Weinberger, P.: Mikrochimica Acta (Wien), Suppl. **6**, 257 (1975); ibid: Berichte der Bunsen-Gessell. für physik. Chem. **79**, 1053 (1975)
18. Neckel, A., Schwarz, K.: Berichte der Bunsen-Gessell. für physik. Chem. **79**, 1071 (1975)
19. Schwarz, K., Hertzig, P.: J. Phys. C. Solid State Physics **12**, 2277 (1979)
20. Electronic Transitions and Optical Properties of Crystals; Bassani and Pastori, Pergamon Press; also see Harrison, W. H., Proceedings of the International Semiconductor Conference, Rome 1976
21. Pople, J. A., Segal, G. A., Santry, D. P.: J. Chem. Phys. **43**, S 129 (1965)
22. Santry, D. P., Segal, G. A.: J. Chem. Phys. **47**, 158 (1967)
23. McAloon, B. J., Perkins, P. G.: Revue Roum. de Chimie **17**, 1813 (1972)
24. O'Shea, S. F., Santry, D. P.: J. Chem. Phys. **54**, 2667 (1971)
25. O'Shea, S. F., Santry, D. P.: Chem. Phys. Letters **28**, 164 (1974)
26. Beveridge, D. J., Jano, I., Ladik, J.: J. Chem. Phys. **56**, 4744 (1972)
27. McAloon, B. J., Perkins, P. G.: J. Chem. Soc. (Faraday II Trans.) **68**, 1121 (1972)
28. McAloon, B. J., Perkins, P. G.: J. Chem. Soc. (Faraday II Trans.) **68**, 1833 (1972).
29. Armstrong, D. R., McAloon, B. J., Perkins, P. G.: J. Chem. Soc. (Faraday II Trans.) **69**, 968 (1973).
30. Harker, A. H., Larkins, F. P.: J. Phys. C. **12**, 2487 (1979)
31. Armstrong, D. R., Perkins, P. G., Stewart, J. J. P.: J. Chem. Soc. **A**, 3674 (1971)
32. Mataga, N., Nishimoto, K.: Z. Physik. Chem. (Frankfurt) **13**, 140 (1957)
33. Fujihara, M., Inokuchi, H.: Chem. Phys. Letters **17**, 554 (1972)
34. Dovesi, R., Pisani, C., Ricca, F., Roetti, C.: J. Chem. Phys. **65**, 3075 (1976)
35. Lomer, W.: Proc. Roy. Soc. (London) **A227**, 330 (1950)
36. Painter, G. S., Ellis, D. E.: Phys. Rev. **B1**, 4747 (1970)
37. Corbato, F. J., in Proceedings of the Third Conference on Carbon (Pergamon, London) 1959, p. 173
38. McFeely, F. R., Kowalczyk, S. P., Ley. L., Cavell, R. G., Pollok, R. R., Shirley, D. A.: Phys. Rev. **B9**, 5268 (1974)
39. Pease, R. S.: Acta Cryst. **5**, 356 (1952).
40. Zunger, A., Katzir, A., Halperin, A.: Phys. Rev. **B13**, 5560 (1976)
41. Perkins, P. G., Wall, D. H.: J. Chem. Soc. **A**, 235 (1966)
42. Rector, C. W., Schaeffer, G. W., Platt, J. R.: J. Chem. Phys. **17**, 460 (1949)
43. Handbook of Chemistry and Physics, Ed. R. C. Weast, Chemical Rubber Publishing Co., Cleveland, Ohio, U.S.A., **56th Ed.**, 1976
44. Painter, G. S., Ellis, D. E., Lubinskey, A. R.: Phys. Rev. **B4**, 3610 (1971)
45. Clark, C. D., Dean, P. J., Harris, P. V.: Proc. Roy. Soc. (London) **A227**, 312 (1964)
46. Pugh, D.: Mol. Phys. **20**, 835 (1971)
47. Wentrof, R. H.: J. Chem. Phys. **26**, 956 (1957)
48. Fomichev, V. A., Runish, M. A.: J. Phys. Chem. Solids **29**, 1025 (1968)
49. Bassani, F., Yoshimine, M.: Phys. Rev. **130**, 20 (1963)
50. Hemstreet, L. A., Fond, C. Y.: Phys. Rev. **B6**, 1464 (1972)
51. Armstrong, D. R., Duke, B. J., Perkins, P. G.: J. Chem. Soc. **A**, 2566 (1969)
52. Armstrong, D. R., Perkins, P. G.: J. Chem. Soc. **A**, 1044 (1969)
53. Levison, K. A., Perkins, P. G.: Theoret. Chim. Acta (Berl.) **14**, 206 (1969)
54. Zupan, J.; Phys. Rev. **B6**, 2477 (1972)
55. Nakhmanson, M. S., Smirnov, V. P.; Soviet Phys.-Solid State, **13**, 754 (1971)

Received January 2, 1980/April 8, 1980